# Enhanced Neural Responses to Self-Name Stimuli Relative to Tone and Reversed Speech Deviants in the Auditory Oddball Paradigm

Fang Duan [*,†] , Xiongping Cao [†] , Zheng Yan , Jianming Chen

Posted Date: 10 April 2026

doi: 10.20944/preprints202604.0678.v1

Keywords: auditory oddball paradigm; event-related potential; source reconstruction; self-referential processing; EEGNet; neural discriminability

*Article*

# Enhanced Neural Responses to Self-Name Stimuli Relative to Tone and Reversed Speech Deviants in the Auditory Oddball Paradigm

**Fang Duan *,†, Xiongping Cao †, Zheng Yan and Jianming Chen**

College of Information Science and Engineering, Huaqiao University, Xiamen, China

* Correspondence: nkfetsh@gmail.com

† These authors contributed equally to this work.

**Abstract**

**Background:** Auditory oddball paradigms are widely used to investigate neural responses to deviant stimuli and attentional processing. However, different paradigms involve deviant stimuli with varying levels of stimulus relevance, and the corresponding neural responses have rarely been directly compared within a unified experimental framework. The aim of this study was to compare neural responses elicited by three variants of the auditory oddball paradigm that differ in the type of deviant stimuli: tone, reversed speech, and self-name deviants. **Methods**: Electroencephalography (EEG) data were recorded from 38 healthy participants while they performed three paradigm variants. Event-related potentials (ERPs) were analyzed to examine neural responses to deviant stimuli. In addition, cortical activation patterns were identified via source reconstruction, and classification analyses were conducted to assess the discriminability of neural responses across the three variants. **Results**: ERP results revealed that the self-name paradigm elicited the most robust neural signatures, characterized by a significant P300 amplitude (3.95 μV) and prominent MMN (-6.39 μV). Crucially, source-space analysis revealed a graded expansion of cortical recruitment: acoustic deviance (tone) and structural reanalysis (reversed speech) were associated with 7 and 6 significant clusters, respectively, primarily in the auditory and fronto-cingulate cortices, whereas the self-name paradigm engaged 12 significant clusters spanning a distributed salience–self network (including the insula and posterior cingulate cortex). Classification analyses mirrored these findings: the self-name paradigm consistently yielding the highest neural separability (~80% accuracy) and greater robustness to interindividual variability, particularly when the EEGNet architecture was used. **Conclusions**: These findings demonstrate that self-referential auditory stimuli elicit stronger and more discriminable neural responses than other auditory deviant stimuli in the oddball paradigm. These results provide a comparative perspective on how different dimensions of auditory relevance modulate neural processing and may inform the design of effective auditory paradigms for cognitive neuroscience and related translational applications.

**Keywords:** auditory oddball paradigm; event-related potential; source reconstruction; self-referential processing; EEGNet; neural discriminability

## 1. Introduction

Auditory perception is a fundamental component of human cognition, supporting the detection of environmental changes and the allocation of attentional resources to behaviorally relevant stimuli[1,2]. One of the most widely used experimental paradigms for investigating these processes is the auditory oddball paradigm, in which infrequent deviant stimuli are embedded in a sequence of frequent standard stimuli[3]. Deviant stimuli typically elicit characteristic neural responses, including event-related potential (ERP) components such as the mismatch negativity (MMN) and

 doi:10.20944/preprints202604.0678.v1



P300, which reflect processes underlying deviance detection, attentional allocation, and stimulus evaluation[4,5].

Variants of the auditory oddball paradigm incorporate deviant stimuli that differ in various stimulus dimensions[6,7]. In the classical tone oddball paradigm, deviant stimuli are typically defined by simple acoustic features (e.g., pitch and frequency)[8–11]. In contrast, speech-based oddball paradigms incorporate deviant stimuli in more complex auditory signals, such as alternations in phonetic structure or speech manipulation[12]. Another line of research has focuses on self-referential stimuli (e.g., one's own name), which are known to have strong attentional and cognitive relevance[13–15]. These distinct types of auditory deviant stimuli engage distinct neural processing pathway via their unique stimulus properties and levels of behavioral relevance[16–18].

Previous studies have extensively investigated neural responses in individual variants of the oddball paradigm[19]. For example, the tone oddball paradigm has been widely used to examine fundamental mechanisms of auditory change detection, whereas speech-based paradigms are commonly used to investigate linguistic and semantic processing[20]. Self-name paradigms have garnered increasing attention due to the high salience of self-related stimuli[21–26]. However, most existing studies focus on a single paradigm variant, and direct comparisons of neural responses to different types of auditory deviant stimuli in a unified experimental framework remain relatively scarce[27–29]. Consequently, it remains unclear how neural responses differ across paradigm variants that vary in terms of stimulus behavioral relevance and complexity.

To address this gap, the present study compared neural responses elicited by three variants of the auditory oddball paradigm that differ in the type of deviant stimuli: tone, reversed speech, and self-name deviants. Electroencephalography (EEG) data were collected from healthy human participants while they completed the three paradigm variants. Event-related potentials (ERPs) were analyzed to characterize neural responses to deviant stimuli. In addition, cortical activation patterns were identified via source reconstruction, and classification analyses were conducted to assess the discriminability of neural responses across the three variants. By comparing these paradigms in a unified experimental design, this study aims to provide a comparative perspective on how different types of auditory deviant stimuli modulate neural responses

## 2. Materials and Methods

### *2.1. Participants*

Thirty-eight healthy right-handed adults (23 males, 15 females; mean age = 23.6 ± 1.9 years) took part in the experiment. All participants were with normal hearing and normal or corrected-to-normal visual acuity, and no self-reported history of neurological or psychiatric disorders. Written informed consent was obtained from all participation prior to study participation, and the study protocol was approved by the Ethics Committee of the School of Medicine, Huaqiao University. Participants were instructed to abstain from caffeine and alcohol on the day of testing and to obtain sufficient rest to ensure high EEG data quality.

### *2.2. Experimental Design and Stimuli*

Three variants of the auditory oddball paradigm (tone, self-name, and reversed speech) were employed to characterize neural responses across acoustic, semantic, and self-referential dimensions, respectively. To ensure high data quality and mitigate participant fatigue, the parameters of each paradigm variant were optimized via pre-experimental pilot tests to maintain a consistent duration of approximately 15 minutes per paradigm, while maximizing the neurophysiological elicitation efficacy for each specific type of variant.The experimental paradigm is shown in Figure 1.

 doi:10.20944/preprints202604.0678.v1



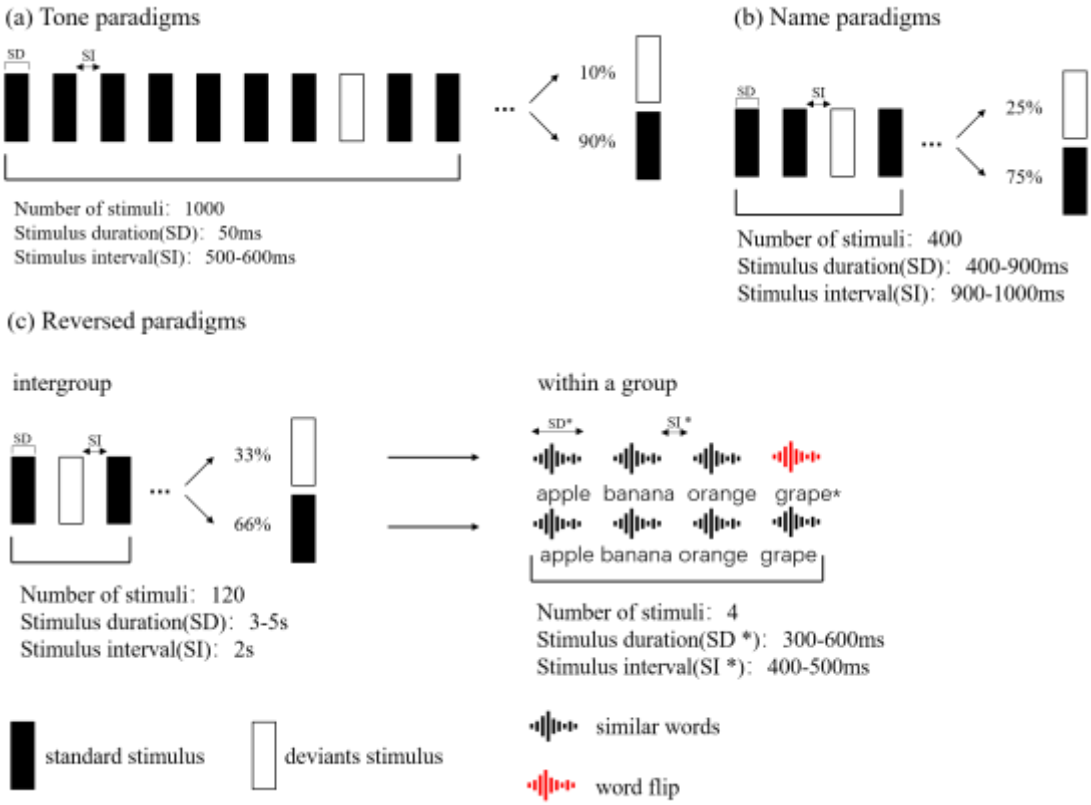


**Figure 1.** This study employed three experimental paradigms: (a) In the Tone paradigm, frequent standard tones (1000 Hz) and infrequent deviant tones (1200 Hz) were presented at a 9:1 ratio under passive listening; (b) In the Name paradigm, unfamiliar names served as standard stimuli and the participant's own name served as the deviant stimulus (3:1 ratio), also under passive listening; (c) In the Reversed paradigm, the deviant stimulus consisted of a polarity-inverted version of the original speech waveform, which preserves acoustic timing but eliminates semantic intelligibility. Participants silently counted the deviant occurrences (2:1 ratio) .

The tone paradigm was designed to assess basic sensory deviance detection. Frequent standard tones (1000 Hz) and infrequent deviant tones (1200 Hz) were presented at a 9:1 ratio (1000 trials total) with a 50ms duration and a 500–600ms interstimulus interval (ISI) under passive listening conditions.

The self-name paradigm was designed to assess self-referential processing. Unfamiliar proper names were used as standard stimuli, whereas each participant's own name was used as the deviant stimulus (3:1 ratio; 400 trials total). Stimuli had a duration of 400–900ms with 900–1000ms ISI under passive listening conditions.

The reversed speech paradigm was designed to probe structural and semantic reanalysis of speech. Each trial consisted of a four-word meaningful semantic sequence, and the final word of the deviant sequence was polarity-inverted. This manipulation preserved the temporal envelope of the speech signal but abolished its semantic intelligibility. The stimuli had a duration of 300–600 ms, with a 400–500 ms ISI within each sequence and a 2000 ms intersequence interval (120 sequences total; 2:1 standard-to-deviant ratio). Unlike the tone and self-name paradigms, which involved passive listening, participants were instructed to silently count the deviant stimuli to maintain a consistent level of attentional engagement, given the higher cognitive load association with semantic processing.

### *2.3. EEG Recording and Preprocessing*

EEG data were recorded using a 68-channel SynAmps² amplifier system (NeuroScan, Charlotte, NC, USA) with Ag/AgCl electrodes placed according to the international 10–20 system. During data acquisition, 62 scalp electrodes were used for subsequent analysis, with peripheral channels, e.g., M1, M2, and EMG, excluded from all analyses. The sampling rate was set to 1000 Hz, and electrode

 doi:10.20944/preprints202604.0678.v1



impedance was kept below 5 kΩ for the entire duration of the experiment. Stimulus presentation and trigger synchronization were controlled using PsychoPy version 2023.2.3, which ensured precise event marking for all standard and deviant trials[30]. The technical route of this study is shown in Figure 2.

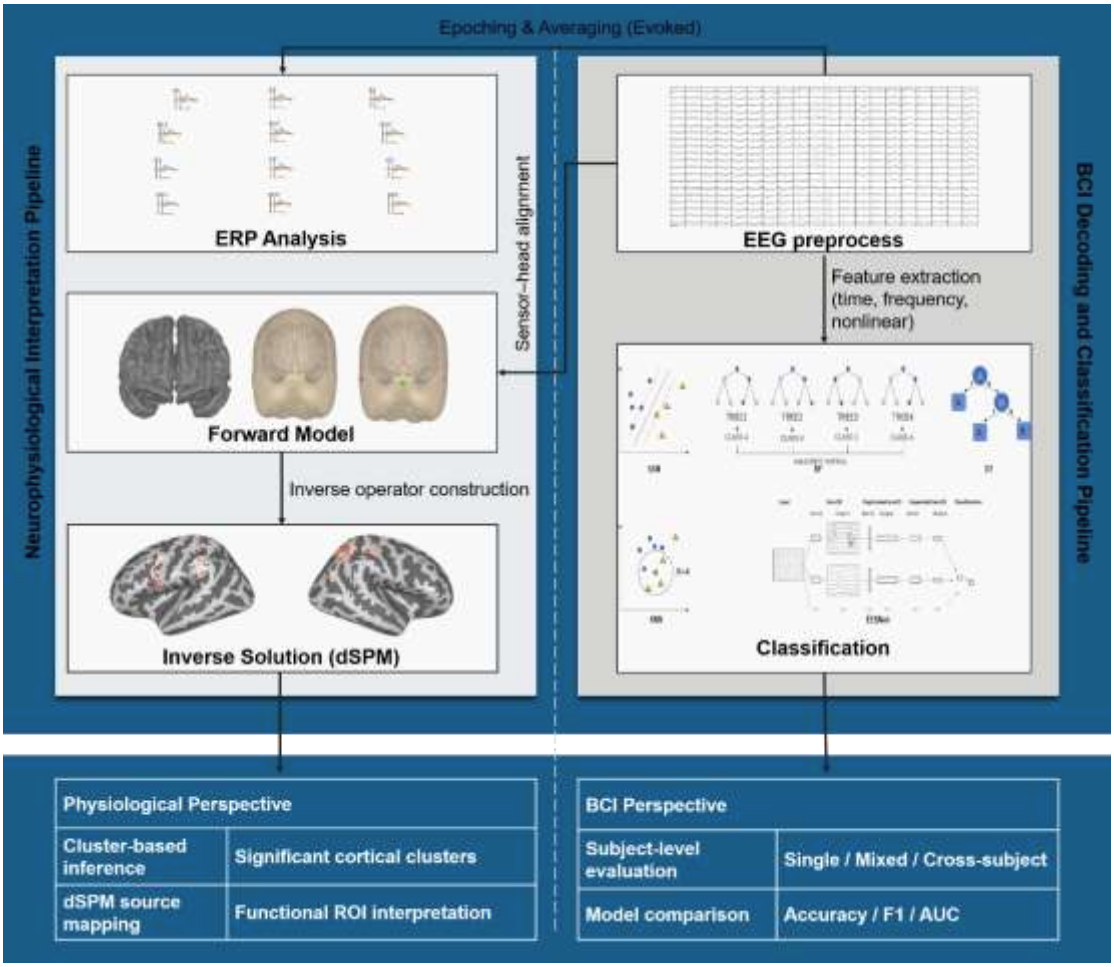


**Figure 2.** EEG data were preprocessed and epoched to obtain evoked responses. Two complementary analysis pipelines were conducted.Left: Neurophysiological interpretation pipeline. Evoked responses were analyzed at the scalp level (ERP analysis), followed by forward modeling and dSPM inverse reconstruction. Significant cortical activations were identified using cluster-based permutation inference, and activation patterns were interpreted at the ROI level.Right: BCI decoding and classification pipeline. Preprocessed EEG segments were used for time-, frequency-, and nonlinear-domain feature extraction, followed by classification using machine-learning (SVM, RF, KNN, DT) and deep-learning (EEGNet) models. Model performance was evaluated at the single-subject, mixed-subject, and cross-subject levels using accuracy, F1, and AUC metrics.Together, the two pipelines provide complementary neurofunctional interpretation and decoding-based discriminability assessment.

EEG preprocessing was performed in Python using the MNE-Python toolbox. Continuous EEG signals were first band-pass filtered from 0.1 to 40 Hz using a zero-phase finite impulse response filter and notch-filtered at 50 Hz to eliminate power-line interference[31]. To establish a neutral reference for subsequent source-space analyses and feature extraction, all scalp EEG data were re-referenced to the common average reference. Independent Component Analysis (ICA) via the FastICA algorithm was subsequently applied to decompose the signals into independent neurophysiological and artifactual components. Artifact identification was conducted by calculating the Pearson correlation coefficients between each independent component and the electrooculography (EOG) channels

 doi:10.20944/preprints202604.0678.v1



(horizontal EOG and vertical EOG). Components that exceeded a predefined correlation threshold, reflecting eye blinks or horizontal eye movements, were identified and systematically removed.

Following artifact correction, the preprocessed EEG data were segmented into epochs time-locked to stimulus onset[32–34]. Baseline correction was applied using the pre-stimulus interval (–100 to 0 ms relative to stimulus onset). To further ensure high data quality, a semi-automated epoch rejection procedure was implemented: electrodes with amplitudes exceeding ±3 standard deviations (SD) from the grand mean were flagged as abnormal, and any epoch containing more than 10% abnormal electrodes was excluded from subsequent analyses. This rigorous screening procedure effectively eliminated residual noise arising from poor electrode contact or transient movement artifacts, ensuring that only high-quality EEG segments were used for neurophysiological interpretation and classification analyses.

### *2.4. Feature Extraction*

To comprehensively characterize neural dynamics across paradigms, EEG features were extracted from three complementary domains: time, frequency, and nonlinear dynamics[35–37]. This multidimensional feature extraction approach was designed to capture both canonical ERP features and the complex, non-stationary temporal patterns underlying auditory processing. The inclusion of nonlinear measures was specifically intended to quantify the increased dynamic signal complexity and stability elicited by highly salient stimuli (e.g., one''s own name), which traditional linear analyses may fail to capture. Random oversampling was applied to balance the class distribution of standard and deviant trials in the model training set.

#### 2.4.1. Time-Domain Features

For each paradigm variant, deviant and standard EEG waveforms were averaged separately, and ERP components were quantified at fronto-central and parietal midline electrodes (Fz, Cz, Pz). Based on typical auditory ERP latencies and the observed grand average waveforms, two temporal analysis windows were defined: an early negative component (50–200 ms relative to stimulus onset, corresponding to Mismatch Negativity, MMN) and a later positive component (200–500 ms; corresponding to P300). For each electrode, the peak amplitude, peak latency, and mean amplitude were extracted within each predefined temporal window. These metrics reflect the temporal magnitude and timing of auditory discrimination and attentional updating processes.

#### 2.4.2. Frequency-Domain Features

Spectral analysis was conducted using a multitaper method to estimate the power spectral density (PSD). The relative power of five canonical EEG frequency bands—delta (1–4 Hz), theta (4–8 Hz), alpha (8–13 Hz), beta (13–30 Hz), and gamma (30–40 Hz)—was calculated for each epoch. To further assess functional neural modulation, band ratio metrics (i.e., $\theta/\alpha$ and $(\delta+\theta)/(\alpha+\beta)$) were calculated, which reflect attentional allocation and arousal state, respectively. These indices reveal paradigm-specific oscillatory characteristics and cognitive load differences across paradigms[38,39].

#### 2.4.3. Nonlinear Features

Given the nonlinear and nonstationary nature of EEG, five complexity metrics were calculated to capture dynamic signal irregularity: Approximate Entropy (ApEn), Sample Entropy (SampEn), Permutation Entropy (PermEn), Spectral Entropy (SpecEn), and Lempel–Ziv Complexity (LZC). Each feature quantifies a distinct aspects of neural complexity and information content, reflecting the diversity and unpredictability of brain activity during stimulus processing. Nonlinear indices were calculated for each electrode and subsequently averaged across all scalp electrode sites to derive global measures for each epoch[40].

By integrating time-, frequency-, and nonlinear-domain features, the present study aimed to characterize both the structured ERP components and the intrinsic dynamic characteristics of the

 doi:10.20944/preprints202604.0678.v1



brain, yielding a comprehensive multiscale feature set for subsequent classification and neurophysiological interpretation.

### *2.5. Classification Analysis*

To assess the discriminability and representational stability of neural responses across paradigms, both traditional machine learning algorithms and a deep-learning framework were employed. The aim was to determine how different dimensions of auditory deviance modulate the separability of standard and deviant trials within a high-dimensional feature space[41].

To assess model robustness and generalizability to interindividual variability, three evaluation schemes were implemented for all classifiers: (1) single-subject evaluation, where models were independently trained and tested for each participant to capture individual-level discriminability; (2) mixed-subject evaluation, which pooled data from all participants to reflect group-level performance; and (3) cross-subject evaluation, which utilized a leave-subject-out partitioning (70% training, 30% testing) to assess the model''s ability to generalize to unseen neural response patterns.

Model performance was quantified using accuracy, precision, recall, F1-score, and the area under the receiver operating characteristic curve (AUC). Given the inherent class imbalance in oddball paradigms, random oversampling was applied to the training set to balance the class distribution of standard and deviant trials, thus rendering accuracy a reliable metric for assessing neural discriminability.

#### 2.5.1. Machine-Learning Models

Four classic machine learning algorithms were employed: Random Forest (RF), Support Vector Machine (SVM), K-Nearest Neighbor (KNN), and Decision Tree (DT). Prior to training, all features were standardized using z-score normalization based on the statistics of the training set. Model hyperparameters were optimized via five-fold cross-validation on the training data to prevent information leakage. The RF consisted of 500 decision trees, the SVM employed a radial basis function kernel, and KNN was set to k = 5 nearest neighbors. Each classifier generated probabilistic outputs corresponding to standard and deviant stimuli.

#### 2.5.2. Deep-Learning Model

For end-to-end feature learning and classification, the EEGNet architecture was adopted as the deep learning model[42]. EEGNet is a compact convolutional neural network specifically designed for EEG-based classification, which uses depthwise and separable convolutions to capture both temporal and spatial neural representations. Input data were band-pass filtered and downsampled to 128 Hz prior to training. The EEGNet model was optimized using the Adam algorithm with a learning rate of 0.001 and cross-entropy loss. Dropout regularization ($p = 0.5$) and early stopping were applied to mitigate model overfitting, and each training session was repeated five times with random weight initialization to ensure reliability.

#### 2.5.3. EEGNet-Based Saliency Analysis

To further elucidate the spatial–temporal neural patterns underlying EEGNet classification, an explainability analysis was conducted using the Integrated Gradients (IG) method. IG quantifies the contribution of each input feature by integrating gradients along a path from a baseline input (all-zero signal) to the actual EEG signal, thereby providing a principled attribution of model predictions.

For each paradigm, IG was computed on correctly classified deviant trials using the trained EEGNet model under the cross-subject evaluation scheme. Attribution maps were calculated at the single-trial level and subsequently averaged across trials and subjects to obtain group-level spatiotemporal representations.

To characterize temporal dynamics, a sliding-window approach (50 ms window width) was applied within the 50–450 ms post-stimulus interval. Within each window, channel-wise attribution

 doi:10.20944/preprints202604.0678.v1



scores were averaged to generate topographical maps. To identify statistically reliable spatial patterns, a non-parametric permutation-based one-sample t-test was performed across subjects for each channel, followed by false discovery rate (FDR) correction ($\alpha = 0.05$). Significant electrodes were marked on the topographic maps to highlight stable discriminative regions contributing to EEGNet classification.

This analysis provides an interpretable link between deep-learning-based decoding performance and underlying neurophysiological processes.

### *2.6. Source-Space Estimation*

To identify the cortical neural generators of ERP components, source-space analysis was performed using the MNE-Python toolbox. A three-layer boundary element model (BEM) was constructed based on the fsaverage standard brain template. Although the use of a template brain introduces anatomical constraints relative to individual MRI-based models, it provides a robust and standardized framework for group-level inference. Conductivity values were set to 0.3 S/m, 0.006 S/m, and 0.3 S/m for the inner skull, outer skull, and scalp compartments, respectively. Electrode positions were co-registered using fiducial landmarks[43,44].

The inverse solution was calculated using dynamic statistical parametric mapping (dSPM) with a loose orientation constraint (0.2) and a signal-to-noise ratio (SNR) set to 3. The noise covariance matrix was estimated from the pre-stimulus baseline interval (–100 to 0 ms). Individual source estimates were morphed to the fsaverage surface for group-level statistical inference. Statistical significance was assessed via a spatio-temporal cluster-based permutation test (5000 permutations, $\alpha = 0.05$). Regions of interest (ROIs) were defined based on the frequency of vertex occurrence within statistically significant clusters to characterize stable cortical activation patterns.

## 3. Results

This section may be divided by subheadings. It should provide a concise and precise description of the experimental results, their interpretation, as well as the experimental conclusions that can be drawn.

### *3.1. ERP Results*

Grand-averaged ERP waveforms across the midline electrodes revealed that all three auditory oddball paradigms successfully elicited a biphasic neural response, consisting of an early negative deflection and a subsequent late positive component. As illustrated in Figure 3, the morphological characteristics of these ERP components were modulated by the type of auditory deviant stimulus. Detailed peak latencies and peak amplitudes for the MMN and P300 components are summarized in Table 1.

**Table 1.** Grand-average ERP Peak Latencies (ms) and Amplitudes (μV) for MMN and P300 Components.

| Paradigm | MMN_Latency | MMN_Amplitude | P300_Latency | P300_Amplitude |
|---|---|---|---|---|
| Tone | 158.0 | -2.30 | 310.0 | 1.77 |
| Name | 205.0 | -6.39 | 371.0 | 3.95 |
| Reversed | 259.0 | -5.67 | 450.0 | 2.55 |

[1] Tables may have a footer.MMN metrics were derived from difference waveforms (deviant minus standard), while P300 metrics were quantified directly from deviant stimulus trials.The unit for the katency indicator is milliseconds, and the unit for the amplitude indicator is microvolts.

 doi:10.20944/preprints202604.0678.v1



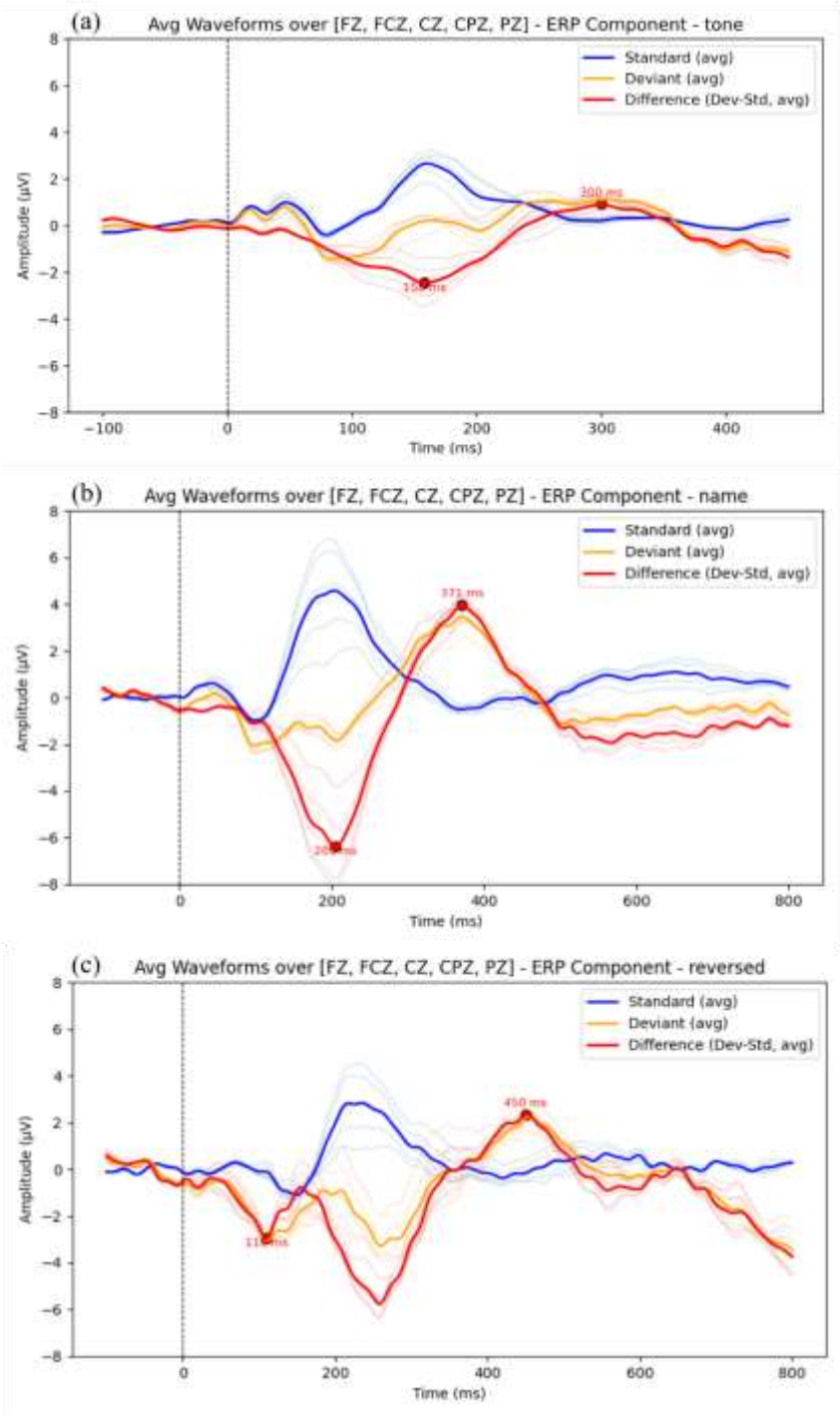


**Figure 3.** Grand-average ERP waveforms across the three auditory paradigms (Tone, Name, Reversed).Evoked responses were averaged across midline electrodes (Fz, FCz, Cz, CPz, Pz). For each paradigm, the standard (blue) and deviant (orange) waveforms are shown along with their difference wave (deviant minus standard; red). Shaded regions indicate ±1 standard error across participants.In the Tone paradigm (a), deviant tones elicited an early negative deflection (~150 ms) followed by a later positive component (~300 ms).In the Name paradigm (b), the participant's own name induced a pronounced late positive component (~370 ms), reflecting enhanced self-relevant processing.In the Reversed paradigm (c), polarity-inverted speech elicited a negative deflection (~255 ms) and a later positive component (~450 ms), indicating preserved acoustic processing with altered semantic integration.The waveforms illustrate paradigm-specific temporal dynamics in auditory deviance processing.

The tone paradigm elicited the smallest and earliest responses, whereas the self-name paradigm induced the most robust neural signatures: the MMN reaching a peak amplitude of -6.39 μV at 205.0

 doi:10.20944/preprints202604.0678.v1



ms and the P300 component reached a peak amplitude of 3.95 μV at 371.0 ms. Although the reversed speech paradigm yeilded higher amplitudes than the tone paradigm, it exhibited the longest peak latencies across all temporal analysis windows, with the P300 component peaking at 450.0 ms. These findings indicate that while acoustic deviance is processed rapidly, self-referential stimuli elicit significantly larger and more robust neural responses.

### *3.2. Source-Space Results*

Source-space estimation via dSPM identified distinct cortical neural generators corresponding to each type of auditory deviant stimulus (Figure 4). Spatio-temporal cluster-based permutation tests revealed varying levels of cortical neural engagement across the three paradigm variants: the tone and reversed speech paradigms yielded 7 and 6 statistically significant clusters, respectively, whereas the self-name paradigm exhibited the most extensive cortical recruitment with 12 significant clusters.The detailed information regarding the number, temporal windows, spatial topography, and statistical values of these significant clusters for each paradigm variant is summarized in Table A1.

Specifically, tone deviant-related cortical activation was primarily localized to the bilateral superior temporal gyrus (STG) during the 150–250 ms post-stimulus interval. Processing of reversed speech deviant stimuli involved the recruitment of the STG, alongside the inferior frontal and cingulate cortices, during the 200–350 ms interval. In contrast, the self-name paradigm demonstrated the most widespread and sustained cortical neural engagement (200–600 ms), with significant clusters extending beyond primary auditory cortices into a distributed salience–self network encompassing the insula and medial parietal cortices. This quantitative increase in significant clusters for the self-name paradigm provides robust empirical evidence for the heightened and prolonged neural salience of self-referential information.

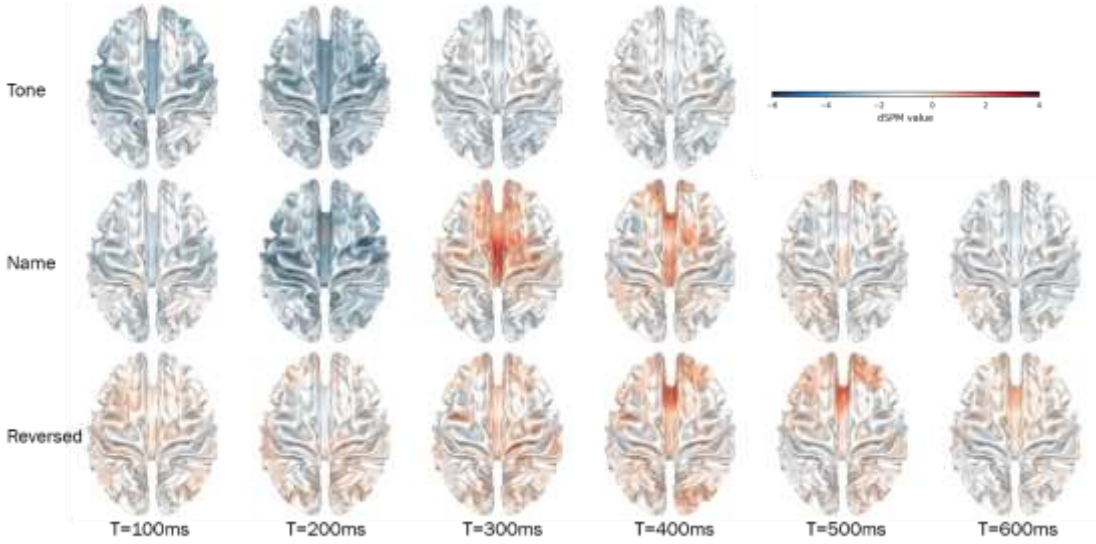


**Figure 4.** Source-level cortical activation across the three auditory paradigms (Tone, Name, Reversed), reconstructed using dSPM and morphed to the fsaverage surface. Each row corresponds to one paradigm, and each column represents a distinct post-stimulus time window. Warmer colors (red) indicate stronger activation in the deviant condition relative to the standard condition, whereas cooler colors (blue) indicate the reverse. The maps highlight paradigm-specific cortical dynamics during auditory deviance processing, with enhanced temporal and frontoparietal engagement for speech-related paradigms (Name and Reversed) relative to the Tone condition.

### *3.3. Classification Results*

All classifiers achieved above-chance classification performance in distinguishing deviant from standard trials across the three paradigm variants. However, decoding accuracy exhibited consistent

 doi:10.20944/preprints202604.0678.v1



differences across both the three paradigm variants and different model types (Figure 5). Across all three evaluation schemes (single-subject, mixed-subject, and cross-subject), the self-name paradigm consistently exhibited the highest decoding performance, followed by the reversed speech and tone paradigms.

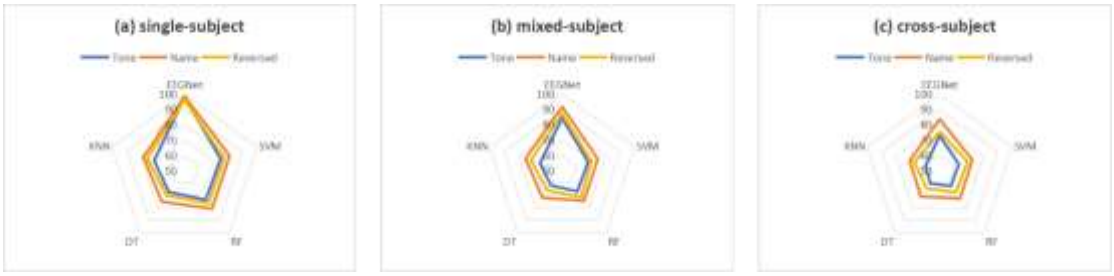


**Figure 5.** Classification performance for the three auditory paradigms (Tone, Name, Reversed) across five classifiers (SVM, RF, DT, KNN, EEGNet) under different evaluation schemes. (a) Single-subject: Models were trained and tested independently for each participant. (b) Mixed-subject: Data from all participants were pooled and randomly divided into training (70%) and testing (30%) sets. (c) Cross-subject: Models were trained on 70% of the participants and evaluated on the remaining 30%, repeated across subject splits. EEGNet consistently achieved the highest classification performance, and the Name paradigm yielded the strongest discriminability across evaluation schemes, followed by Reversed and Tone.

Among the five classifiers tested, the EEGNet model achieved the best overall classification performance and demonstrated greater robustness to interindividual variability, particularly in the cross-subject condition. Among traditional machine learning models, SVM showed the most stable and competitive performance, whereas the RF, KNN, and DT models yielded comparatively lower classification accuracies.

Classification performance generally decreased as interindividual variability increased (i.e., single-subject > mixed-subject > cross-subject); however, the relative ranking of paradigm variants and classifiers remained unchanged. These results indicate that semantic and self-referential processing of auditory stimuli enhances the discriminability of neural responses, thereby improving EEG-based auditory deviance decoding performance.

### *3.4. EEGNet Saliency Topography*

To further interpret the neural features driving EEGNet classification, spatiotemporal saliency maps derived from Integrated Gradients were analyzed as shown in Figure 6.

Across all three paradigms, discriminative neural patterns exhibited clear temporal evolution within the 50–450 ms post-stimulus interval. In the tone paradigm, salient activity was primarily confined to early time windows (50–150 ms), with spatial contributions localized to fronto-central regions. The overall saliency magnitude was relatively weak and spatially sparse, indicating that EEGNet relied on limited early sensory features for classification.

In contrast, the reversed speech paradigm demonstrated a broader temporal engagement, with salient patterns emerging from approximately 100 ms and extending into later stages (~350 ms). Spatially, these contributions involved both fronto-central and parietal regions, reflecting increased processing demands associated with structural reanalysis of speech.

The self-name paradigm exhibited the most prominent and sustained saliency patterns. Strong and widespread contributions were observed from 150 ms onward, peaking within the 200–400 ms interval. Notably, significant electrodes were distributed across fronto-central and parietal regions, consistent with the canonical P300 topography. Compared to the other paradigms, the self-name condition showed both higher saliency magnitude and greater spatial extent.

Importantly, the temporal windows showing maximal saliency closely aligned with ERP components identified in Section 3.1, particularly the MMN and P300 intervals. Furthermore, the

 doi:10.20944/preprints202604.0678.v1



spatial distribution of salient electrodes corresponded with cortical regions identified in source-space analysis (Section 3.2), suggesting that EEGNet classification is primarily driven by neurophysiologically meaningful patterns rather than spurious features.

Collectively, these results indicate that increasing stimulus relevance enhances not only neural response amplitude but also the stability and spatial extent of discriminative neural representations captured by deep learning models.

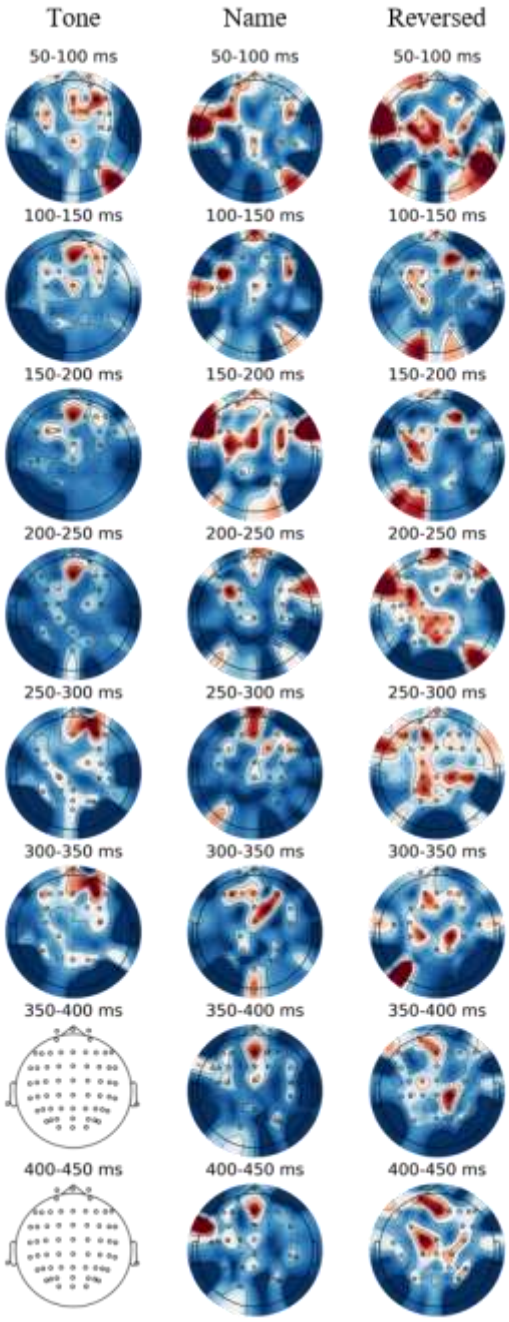


**Figure 6.** EEGNet saliency topography across paradigms. Spatiotemporal saliency topographies derived from EEGNet using Integrated Gradients across the three auditory paradigms (Tone, Reversed, Name). Each row represents a time window (50 ms sliding window), and each column corresponds to a paradigm. Warmer colors indicate higher attribution values. Electrodes marked with circles denote statistically significant contributions after FDR correction ($\alpha$ = 0.05). The results reveal progressively stronger and more spatially distributed discriminative patterns from tone to self-name paradigms, particularly within the 200–400 ms interval.

 doi:10.20944/preprints202604.0678.v1



## 4. Discussion

The present study compared neural responses across three variants of the auditory oddball paradigm that differed in the type of deviant stimuli: tone, reversed speech, and self-name deviants. All three paradigm variants elicited robust neural responses to deviant stimuli, confirming the effectiveness of the auditory oddball paradigm for investigating auditory change detection[45,46]. However, notable differences in neural response were observed across the three paradigms. The self-name condition produced larger P300 amplitudes, more extensive cortical activation patterns, and higher classification accuracy compared with the tone and reversed speech conditions. In particular, the P300 amplitude in the self-name condition was approximately 3.9 μV, whereas the tone condition elicited a markedly smaller response of approximately 1.8 μV. These findings demonstrate that self-referential auditory stimuli elicit stronger and more discriminable neural responses than other types of auditory deviant stimuli.

These observed differences across the three paradigm variants may be attributed to the distinct intrinsic characteristics of the deviant stimuli. In the tone oddball paradigm, deviant stimuli are typically defined by simple acoustic changes (e.g., frequency differences). This paradigm primarily engages the basic neural mechanisms of auditory change detection and has been widely used to investigate early stages of auditory sensory processing[47]. In contrast, the reversed speech paradigm incorporates deviant stimuli in more complex auditory speech signals, which requires additional structural and semantic reanalysis of speech. Detecting such deviations may involve more extensive auditory cognitive processing beyond simple acoustic discrimination. The self-name paradigm involves a unique type of deviant stimulus that carries strong personal and self-referential relevance. Processing one''s own name is known to capture automatic attentional resource and elicit enhanced neural responses, even under conditions of limited attentional resources. Consistent with previous research findings, the present results showed that self-name stimuli yielded the largest P300 responses among the three paradigm variants, indicating attentional engagement with self-referential stimuli.

Beyond the observed ERP differences, the classification analysis further confirmed that neural responses to self-name stimuli were more readily distinguishable from those to standard stimuli[48]. Classification accuracy in the self-name condition reached approximately 80%, which was markedly higher than that in the tone and reversed speech paradigms. This finding indicates that self-referential auditory stimuli elicit neural responses with significantly higher discriminability. From a methodological perspective, this unique characteristic of self-referential stimuli has important practical implications for the design of effective auditory paradigms in cognitive neuroscience research and related applications. Auditory paradigms that incorporate stimuli with higher behavioral and self-referential relevance may enhance the robustness of neural responses and improve the detectability of deviant stimulus-related neural activity.

To further bridge the gap between neural representation and model performance, the EEGNet-based saliency analysis provides critical insights into the features underlying successful classification. The saliency maps revealed that EEGNet predominantly relied on temporally and spatially structured neural activity rather than diffuse or noise-driven patterns.

Specifically, the alignment between saliency peaks and canonical ERP components (MMN and P300) suggests that the model implicitly captures well-established neurophysiological signatures of auditory deviance processing. Moreover, the spatial distribution of salient electrodes, particularly the fronto-central and parietal regions observed in the self-name paradigm, is highly consistent with the scalp topography of attentional and self-referential processing.

Importantly, the progressive increase in saliency strength and spatial extent from tone to reversed speech to self-name paradigms mirrors the hierarchy observed in ERP amplitude, source-level activation, and classification performance. This convergence across analytical levels supports the interpretation that enhanced behavioral relevance leads to more robust, spatially coherent, and temporally stable neural representations, which are more readily captured by deep learning models.

 doi:10.20944/preprints202604.0678.v1



From a methodological perspective, these findings highlight that EEGNet does not function as a "black box" but rather extracts physiologically meaningful features that correspond to known cognitive processes. The integration of explainability analysis thus strengthens the interpretability of decoding results and provides a mechanistic link between neural dynamics and classification performance.

Several limitations of the present study should be acknowledged when interpreting its findings. First, the three paradigm variants differed in multiple stimulus properties, including acoustic characteristics and behavioral relevance of the deviant stimuli. Therefore, the present study does not constitute a strictly controlled comparison of stimulus complexity across conditions. Instead, the results should be interpreted as a comparative analysis of commonly used variants of the auditory oddball paradigm that differ in the type of deviant stimuli. Second, the present study only included healthy young adult participants, and the generalizability of its findings to other populations (e.g., clinical populations, older adults) remains to be explored. Future research could further explore the neural response elicited by different auditory oddball paradigm variants in clinical populations, as well as in studies investigating attentional modulation and conscious perception.

## 5. Conclusions

The present study compared neural responses across three variants of the auditory oddball paradigm, which incorporated tone, reversed speech, and self-name deviant stimuli. All three paradigm variants successfully elicited robust deviant stimulus-related neural responses, demonstrating the effectiveness of the auditory oddball paradigm design for investigating auditory change detection in the human brain.

Among the three paradigms, self-name stimuli yielded significantly larger P300 amplitudes, more extensive cortical activation patterns, and higher classification accuracy than tone and reversed speech deviant stimuli. These findings suggest that self-referential auditory stimuli may elicit significantly stronger and more discriminable neural responses in the auditory oddball paradigm. These results provide a valuable comparative perspective on neural responses to different types of auditory deviant stimuli and contribute to the selection and design of effective auditory oddball paradigms for cognitive neuroscience research and translational applications. Importantly, the convergence of ERP, source-space, classification, and saliency analyses provides a multi-level validation framework, demonstrating that deep learning models capture neurophysiologically grounded representations of auditory salience.

**Author Contributions:** Conceptualization, F.D., X.C. and J.C.; methodology, F.D.and X.C.; software, X.C.; validation, X.C. and F.D.; formal analysis, X.C. and J.C.; investigation, X.C.and F.D.; resources, F.D. and Z.Y.; data curation, X.C.; writing—original draft preparation, F.D.and X.C.; writing—review and editing, F.D.and X.C.; visualization, X.C.; supervision, F.D. and Z.Y.; project administration, F.D. and Z.Y.; funding acquisition, F.D. and Z.Y. All authors have read and agreed to the published version of the manuscript.

**Funding:** This work is partially supported by Open Foundation of Engineering Research Center of Big Data Application in Private Health Medicine, Fujian Province University (MKF202203).

**Institutional Review Board Statement:** This study was performed in line with the principles of the Declaration of Helsinki. Approval was granted by the Medical Ethics Committee of the Faculty of Medicine of Huaqiao University (No. M2021013, 21 April 2021).

**Informed Consent Statement:** Informed consent was obtained from all subjects involved in this study. Written informed consent has been obtained from the patient(s) to publish this paper.

**Data Availability Statement:** The data supporting this study's findings are available on request with the consent of the corresponding authors F.D. However, the data are not publicly available because they contain information that could compromise the privacy of research participants.

**Conflicts of Interest:** The authors declare no conflicts of interest.

 doi:10.20944/preprints202604.0678.v1



## Appendix A

Appendix A here is the result from the source space analysis obtained through permutation test.

**Table A1.** Summary of significant spatio-temporal clusters for Tone, Reversed, and Name paradigms.

| Paradigm | Cluster ID | Time Range (ms) | Vertices | p-value | Primary Regions |
|---|---|---|---|---|---|
| Tone | 0 | 1.0 - 395.0 | 3889 | 0.0003 | superiorfrontal-lh: 278 (7.1%); precentral-lh: 256 (6.6%); superiorparietal-lh: 239 (6.1%); postcentral-lh: 202 (5.2%); rostralmiddlefrontal-lh: 201 (5.2%) |
| | 1 | 5.0 - 450.0 | 3748 | 0.0003 | inferiorparietal-rh : 241 (6.4%); superiorfrontal-rh : 238 (6.4%); superiorparietal-rh : 229 (6.1%); precentral-rh : 220 (5.9%); rostralmiddlefrontal-rh : 197 (5.3%) |
| | 2 | 37.0 - 107.0 | 97 | 0.0180 | superiorparietal-lh : 50 (51.5%); lateraloccipital-lh : 26 (26.8%); inferiorparietal-lh : 21 (21.6%) |
| | 3 | 134.0 - 208.0 | 52 | 0.0233 | superiorparietal-rh : 40 (76.9%); inferiorparietal-rh : 12 (23.1%) |
| | 4 | 351.0 - 398.0 | 70 | 0.0410 | inferiorparietal-rh : 35 (50.0%); superiorparietal-rh : 35 (50.0%) |
| | 5 | 360.0 - 450.0 | 1920 | 0.0007 | precentral-lh : 159 (8.3%); superiortemporal-lh : 140 (7.3%); insula-lh : 118 (6.1%); postcentral-lh : 107 (5.6%); precuneus-lh : 100 (5.2%) |
| | 6 | 401.0 - 430.0 | 74 | 0.0350 | superiorparietal-rh : 74 (100.0%) |
| Name | 0 | 322.0 - 397.0 | 61 | 0.0127 | lateralorbitofrontal-lh : 5 (8.2%); medialorbitofrontal-lh : 1 (1.6%) |
| | 1 | 34.0 - 101.0 | 117 | 0.0167 | insula-lh : 64 (54.7%) parstriangularis-lh : 20 (17.1%); parsopercularis-lh : 11 (9.4%); superiortemporal-lh : 9 (7.7%); supramarginal-lh : 8 (6.8%) |

 doi:10.20944/preprints202604.0678.v1



| | | | | |
|---|---|---|---|---|
| 2 | 49.0 - 118.0 | 69 | 0.0260 | supramarginal-rh : 43 (62.3%); postcentral-rh : 16 (23.2%); insula-rh : 9 (13.0%); precentral-rh : 1 (1.4%) |
| 3 | 134.0 - 208.0 | 151 | 0.0083 | posteriorcingulate-lh : 48 (31.8%); caudalanteriorcingulate-lh : 7 (4.6%); isthmuscingulate-lh : 2 (1.3%) |
| 4 | 60.0 - 114.0 | 120 | 0.0153 | posteriorcingulate-rh : 22 (18.3%); caudalanteriorcingulate-rh : 12 (10.0%); rostralanteriorcingulate-rh : 1 (0.8%) |
| 5 | 111.0 - 270.0 | 1913 | 0.0003 | superiortemporal-rh : 128 (6.7%); precentral-rh : 117 (6.1%); precuneus-rh : 111 (5.8%); superiorparietal-rh : 106 (5.5%); supramarginal-rh : 101 (5.3%) |
| 6 | 121.0 - 265.0 | 1974 | 0.0003 | precentral-lh : 211 (10.7%); postcentral-lh : 171 (8.7%); superiorfrontal-lh : 117 (5.9%); superiortemporal-lh : 111 (5.6%); precuneus-lh : 109 (5.5%) |
| 7 | 151.0 - 249.0 | 30 | 0.0340 | inferiorparietal-rh : 30 (100.0%) |
| 8 | 153.0 - 235.0 | 22 | 0.0367 | precentral-rh : 22 (100.0%) |
| 9 | 630.0 - 764.0 | 44 | 0.0150 | precentral-lh : 21 (47.7%); parsopercularis-lh : 14 (31.8%); caudalmiddlefrontal-lh : 8 (18.2%); rostralmiddlefrontal-lh : 1 (2.3%) |
| 10 | 630.0 - 706.0 | 70 | 0.0443 | insula-rh : 46 (65.7%); supramarginal-rh : 13 (18.6%); postcentral-rh : 7 (10.0%); superiortemporal-rh : 3(4.3%); precentral-rh : 1 (1.4%) |
| 11 | 675.0 - 707.0 | 106 | 0.0170 | medialorbitofrontal-rh : 5 (4.7%); rostralanteriorcingulate-rh : 1 (0.9%) |

 doi:10.20944/preprints202604.0678.v1



| | | | | | |
|---|---|---|---|---|---|
| Reversed | 0 | 422.0 - 508.0 | 46 | 0.0137 | caudalanteriorcingulate-lh : 29 (63.0%); rostralanteriorcingulate-lh : 6 (13.0%); posteriorcingulate-lh : 3 (6.5%); superiorfrontal-lh : 2 (4.3%) |
| | 1 | 724.0 - 800.0 | 58 | 0.0100 | none |
| | 2 | 730.0 - 800.0 | 41 | 0.0180 | posteriorcingulate-rh : 27 (65.9%); precuneus-rh : 14 (34.1%) |
| | 3 | 731.0 - 800.0 | 53 | 0.0037 | posteriorcingulate-lh : 22 (41.5%); isthmuscingulate-lh : 12 (22.6%); caudalanteriorcingulate-lh : 1 (1.9%) |
| | 4 | 733.0 - 808.0 | 120 | 0.0023 | posteriorcingulate-rh : 24 (20.0%); isthmuscingulate-rh : 16 (13.3%); caudalanteriorcingulate-rh : 2 (1.7%) |
| | 5 | 205.0 - 275.0 | 35 | 0.0283 | precentral-rh : 31 (88.6%); caudalmiddlefrontal-rh : 2 (5.7%); parsopercularis-rh : 2 (5.7%) |

## References


1. Näätänen, R.; Paavilainen, P.; Rinne, T.; Alho, K. The mismatch negativity (MMN) in basic research of central auditory processing: A review. *Clinical Neurophysiology* **2007**, *118*, 2544-2590, doi:10.1016/j.clinph.2007.04.026.
2. Polich, J. Updating P300: An integrative theory of P3a and P3b. *Clinical Neurophysiology* **2007**, *118*, 2128-2148, doi:10.1016/j.clinph.2007.04.019.
3. Garrido, M.I.; Kilner, J.M.; Stephan, K.E.; Friston, K.J. The mismatch negativity: A review of underlying mechanisms. *Clinical Neurophysiology* **2009**, *120*, 453-463, doi:10.1016/j.clinph.2008.11.029.
4. Doeller, C.F.; Opitz, B.; Mecklinger, A.; Krick, C.; Reith, W.; Schröger, E. Prefrontal cortex involvement in preattentive auditory deviance detection. *NeuroImage* **2003**, *20*, 1270-1282, doi:10.1016/s1053-8119(03)00389-6.
5. Opitz, B.; Rinne, T.; Mecklinger, A.; von Cramon, D.Y.; Schröger, E. Differential Contribution of Frontal and Temporal Cortices to Auditory Change Detection: fMRI and ERP Results. *NeuroImage* **2002**, *15*, 167-174, doi:10.1006/nimg.2001.0970.
6. Liu, Y.; Li, P.; Shu, H.; Zhang, Q.; Chen, L. Structure and meaning in Chinese: An ERP study of idioms. *Journal of Neurolinguistics* **2010**, *23*, 615-630, doi:10.1016/j.jneuroling.2010.06.001.
7. Schnakers, C.; Perrin, F.; Schabus, M.; Majerus, S.; Ledoux, D.; Damas, P.; Boly, M.; Vanhaudenhuyse, A.; Bruno, M.A.; Moonen, G.; et al. Voluntary brain processing in disorders of consciousness. *Neurology* **2008**, *71*, 1614-1620, doi:10.1212/01.wnl.0000334754.15330.69.
8. Alexopoulos, T.; Muller, D.; Ric, F.; Marendaz, C. I, me, mine: Automatic attentional capture by self-related stimuli. *European Journal of Social Psychology* **2012**, *42*, 770-779, doi:10.1002/ejsp.1882.
9. Höller, Y.; Kronbichler, M.; Bergmann, J.; Crone, J.S.; Ladurner, G.; Golaszewski, S. EEG frequency analysis of responses to the own-name stimulus. *Clinical Neurophysiology* **2011**, *122*, 99-106, doi:10.1016/j.clinph.2010.05.029.

 doi:10.20944/preprints202604.0678.v1




10. Näätänen, R.; Kujala, T.; Winkler, I. Auditory processing that leads to conscious perception: A unique window to central auditory processing opened by the mismatch negativity and related responses. *Psychophysiology* **2010**, *48*, 4-22, doi:10.1111/j.1469-8986.2010.01114.x.
11. Thornhill, D.E.; Van Petten, C. Lexical versus conceptual anticipation during sentence processing: Frontal positivity and N400 ERP components. *International Journal of Psychophysiology* **2012**, *83*, 382-392, doi:10.1016/j.ijpsycho.2011.12.007.
12. Qin, P.; Di, H.; Yan, X.; Yu, S.; Yu, D.; Laureys, S.; Weng, X. Mismatch negativity to the patient's own name in chronic disorders of consciousness. *Neuroscience Letters* **2008**, *448*, 24-28, doi:10.1016/j.neulet.2008.10.029.
13. Ghani, U.; Signal, N.; Niazi, I.K.; Taylor, D. ERP based measures of cognitive workload: A review. *Neuroscience & Biobehavioral Reviews* **2020**, *118*, 18-26, doi:10.1016/j.neubiorev.2020.07.020.
14. Hsu, Y.F.; Darriba, A.; Waszak, F. Attention modulates repetition effects in a context of low periodicity. *Brain Res* **2021**, *1767*, 147559, doi:10.1016/j.brainres.2021.147559.
15. Orban, M.; Elsamanty, M.; Guo, K.; Zhang, S.; Yang, H. A Review of Brain Activity and EEG-Based Brain–Computer Interfaces for Rehabilitation Application. *Bioengineering* **2022**, *9*, 768, doi:10.3390/bioengineering9120768.
16. Blankertz, B.; Lemm, S.; Treder, M.; Haufe, S.; Müller, K.-R. Single-trial analysis and classification of ERP components — A tutorial. *NeuroImage* **2011**, *56*, 814-825, doi:10.1016/j.neuroimage.2010.06.048.
17. Gilmore, C.S.; Clementz, B.A.; Berg, P. Hemispheric differences in auditory oddball responses during monaural versus binaural stimulation. *International Journal of Psychophysiology* **2009**, *73*, 326-333, doi:10.1016/j.ijpsycho.2009.05.005.
18. Qin, P.; Northoff, G. How is our self related to midline regions and the default-mode network? *NeuroImage* **2011**, *57*, 1221-1233, doi:10.1016/j.neuroimage.2011.05.028.
19. Brown, A.; Pinto, D.; Burgart, K.; Zvilichovsky, Y.; Zion-Golumbic, E. Neurophysiological Evidence for Semantic Processing of Irrelevant Speech and Own-Name Detection in a Virtual Café. *The Journal of Neuroscience* **2023**, *43*, 5045-5056, doi:10.1523/jneurosci.1731-22.2023.
20. Erlbeck, H.; Real, R.G.L.; Kotchoubey, B.; Mattia, D.; Bargak, J.; Kübler, A. Basic discriminative and semantic processing in patients in the vegetative and minimally conscious state. *International Journal of Psychophysiology* **2017**, *113*, 8-16, doi:10.1016/j.ijpsycho.2016.12.012.
21. Holeckova, I.; Fischer, C.; Giard, M.-H.; Delpuech, C.; Morlet, D. Brain responses to a subject''s own name uttered by a familiar voice. *Brain Research* **2006**, *1082*, 142-152, doi:10.1016/j.brainres.2006.01.089.
22. Huang, F.; Wu, J.; Cheng, L.; Meng, Y. The Effects of Synonym and Antonym Relations on Visual Recognition of Chinese Compound Words: Based on Behavioral and ERP Experiments. *International Journal of Psychophysiology* **2021**, *168*, doi:10.1016/j.ijpsycho.2021.07.327.
23. Nijhof, A.D.; von Trott Zu Solz, J.; Catmur, C.; Bird, G. Equivalent own name bias in autism: An EEG study of the Attentional Blink. *Cogn Affect Behav Neurosci* **2022**, *22*, 625-639, doi:10.3758/s13415-021-00967-w.
24. Roer, J.P.; Cowan, N. A preregistered replication and extension of the cocktail party phenomenon: One''s name captures attention, unexpected words do not. *J Exp Psychol Learn Mem Cogn* **2021**, *47*, 234-242, doi:10.1037/xlm0000874.
25. Wu, H.; Wang, D.; Liu, Y.; Xie, M.; Zhou, L.; Wang, Y.; Cao, J.; Huang, Y.; Qiu, M.; Qin, P. Decoding subject''s own name in the primary auditory cortex. *Human Brain Mapping* **2022**, *44*, 1985-1996, doi:10.1002/hbm.26186.
26. Zhang, Y.; Xie, M.; Wang, Y.; Qin, P. Distinct Effects of Stimulus Repetition on Various Temporal Stages of Subject's Own Name Processing. *Brain Sciences* **2022**, *12*, 411.
27. Bao, H.; Xie, M.; Huang, Y.; Liu, Y.; Lan, C.; Lin, Z.; Wang, Y.; Qin, P. Specificity in the processing of a subject's own name. *Social Cognitive and Affective Neuroscience* **2023**, *18*, nsad066, doi:10.1093/scan/nsad066.
28. Tamura, K.; Mizuba, T.; Iramina, K. ERP and time-frequency analysis of the response to hearing subject''s own name. *International Journal of Psychophysiology* **2014**, *94*, doi:10.1016/j.ijpsycho.2014.08.677.
29. Wang, F.; Di, H.; Hu, X.; Jing, S.; Thibaut, A.; Di Perri, C.; Huang, W.; Nie, Y.; Schnakers, C.; Laureys, S. Cerebral response to subject's own name showed high prognostic value in traumatic vegetative state. *BMC Medicine* **2015**, *13*, 83, doi:10.1186/s12916-015-0330-7.

 doi:10.20944/preprints202604.0678.v1




30. Gramfort, A.; Luessi, M.; Larson, E.; Engemann, D.A.; Strohmeier, D.; Brodbeck, C.; Parkkonen, L.; Hämäläinen, M.S. MNE software for processing MEG and EEG data. *NeuroImage* **2014**, *86*, 446-460, doi:10.1016/j.neuroimage.2013.10.027.
31. Liu, Y.; Huang, C.; Huang, X.; Chen, H.; Qin, P. Using the attribute amnesia paradigm to test the automatic memory advantage of person names. *Psychon Bull Rev* **2021**, *28*, 2019-2026, doi:10.3758/s13423-021-01975-0.
32. Guan, L.; Qi, M.; Li, H.; Hitchman, G.; Yang, J.; Liu, Y. Priming with threatening faces modulates the self-face advantage by enhancing the other-face processing rather than suppressing the self-face processing. *Brain Res* **2015**, *1608*, 97-107, doi:10.1016/j.brainres.2015.03.002.
33. Hervais-Adelman, A.G.; Carlyon, R.P.; Johnsrude, I.S.; Davis, M.H. Brain regions recruited for the effortful comprehension of noise-vocoded words. *Language and Cognitive Processes* **2012**, *27*, 1145-1166, doi:10.1080/01690965.2012.662280.
34. Real, R.G.L.; Veser, S.; Erlbeck, H.; Risetti, M.; Vogel, D.; Müller, F.; Kotchoubey, B.; Mattia, D.; Kübler, A. Information processing in patients in vegetative and minimally conscious states. *Clinical Neurophysiology* **2016**, *127*, 1395-1402, doi:10.1016/j.clinph.2015.07.020.
35. Fan, X.; Han, S. Neural responses to one''s own name under mortality threat. *Neuropsychologia* **2018**, *108*, 32-41, doi:10.1016/j.neuropsychologia.2017.11.026.
36. Honbolygó, F.; Zulauf, B.; Zavogianni, M.I.; Csépe, V. Investigating the neurocognitive background of speech perception with a fast multi-feature MMN paradigm. *Biologia Futura* **2024**, *75*, 145-158, doi:10.1007/s42977-024-00219-1.
37. Li, Y.; Peng, P.; Guo, T.; Lu, P.; Liu, X.; Chen, S.; Liu, L.; Guo, T. A Comparison Between the Oddball Paradigm and the Multi-Feature Paradigm: Evidence From an Event-Related Potential Study on Processing Mandarin Vowels and Tones. *European Journal of Neuroscience* **2025**, *62*, e70212, doi:https://doi.org/10.1111/ejn.70212.
38. Apps, M.A.; Tsakiris, M. The free-energy self: a predictive coding account of self-recognition. *Neurosci Biobehav Rev* **2014**, *41*, 85-97, doi:10.1016/j.neubiorev.2013.01.029.
39. Takasago, M.; Kunii, N.; Fujitani, S.; Ishishita, Y.; Tada, M.; Kirihara, K.; Komatsu, M.; Uka, T.; Shimada, S.; Nagata, K.; et al. Auditory prediction errors in sound frequency and duration generated different cortical activation patterns in the human brain: an ECoG study. *Cerebral Cortex* **2024**, *34*, bhae072, doi:10.1093/cercor/bhae072.
40. Carter, J.A.; Bidelman, G.M. Perceptual warping exposes categorical representations for speech in human brainstem responses. *NeuroImage* **2023**, *269*, 119899, doi:https://doi.org/10.1016/j.neuroimage.2023.119899.
41. Saparbayeva, M.; Shomanov, A.; Lee, M.-H. A Novel Binary BCI Systems Based on Non-oddball Auditory and Visual Paradigms. Cham, 2021; pp. 3-14.
42. Lawhern, V.J.; Solon, A.J.; Waytowich, N.R.; Gordon, S.M.; Hung, C.P.; Lance, B.J. EEGNet: A Compact Convolutional Network for EEG-based Brain-Computer Interfaces. *Journal of Neural Engineering* **2018**, *15*, 056013.056011-056013.056017.
43. Hauk, O.; Stenroos, M.; Treder, M.S. Towards an objective evaluation of EEG/MEG source estimation methods – The linear approach. *NeuroImage* **2022**, *255*, 119177, doi:https://doi.org/10.1016/j.neuroimage.2022.119177.
44. Yazıcı, M.; Ulutaş, M.; Okuyan, M. Effect of EEG Electrode Numbers on Source Estimation in Motor Imagery. *Brain Sciences* **2025**, *15*, 685, doi:10.3390/brainsci15070685.
45. Deroche, M.L.D.; Wolfe, J.; Neumann, S.; Manning, J.; Towler, W.; Alemi, R.; Bien, A.G.; Koirala, N.; Hanna, L.; Henry, L.; et al. Auditory evoked response to an oddball paradigm in children wearing cochlear implants. *Clinical Neurophysiology* **2023**, *149*, 133-145, doi:10.1016/j.clinph.2023.02.179.
46. Jiang, C.G.; Wang, J.; Sun, Y.F.; Tan, S.P.; Percell, S.M.; Zhou, Z.H.; Pan, J.Q.; Hall, M.H.; consortium, G. Unveiling distinct representations of P3a in schizophrenia through two-stimulus and three-stimulus auditory oddball paradigms. *Schizophrenia Research* **2025**, *277″″″*, 159-168, doi:10.1016/j.schres.2025.03.004.

 doi:10.20944/preprints202604.0678.v1



47. Pruvost-Robieux, E.; Benghanem, S.; Lauriers, C.D.; Llorens, A.; Gavaret, M. How can emotion and familiarity improve own-name oddball paradigms? *Neurophysiologie Clinique* **2025**, *55*, 103050, doi:https://doi.org/10.1016/j.neucli.2025.103050.
48. Yang, Y.; An, X.; Chen, L.; Liu, S.; Zhao, X.; Ming, D. Study on the effect of nontarget types on name based auditory event-related potentials. *Annu Int Conf IEEE Eng Med Biol Soc* **2020**, *2020*, 3003-3006, doi:10.1109/EMBC44109.2020.9176350.